

# High temperature superconducting RF coil fabrication on flexible ceramic substrates for magnetic resonance imaging applications

(PN-III-P1-1.1-TE-2019-1777, Contract Nr. 191/2021)

## Scientific Report I

### Contents

Summary .....	1
1. Solution deposition planarization of flexible, ceramic YSZ substrates.....	2
A1.1 Coating solution synthesis and characterization .....	2
A1.3 Optimization of the double-sided deposition process by dip-coating.....	3
A1.4 Morphologic characterization of the planarization layers.....	4
Results and perspectives .....	4
2. YBCO thin film deposition (A2.7/8) .....	5
2.1 Experimental .....	5
2.2 Infrared spectroscopy characterization of the precursor solution .....	6
2.3 Thermal decomposition of precursor powders.....	7
2.4 Structural and morphological characterization.....	9
2.5 Superconducting transport properties.....	11
Results and perspectives .....	15
3. Dissemination.....	15

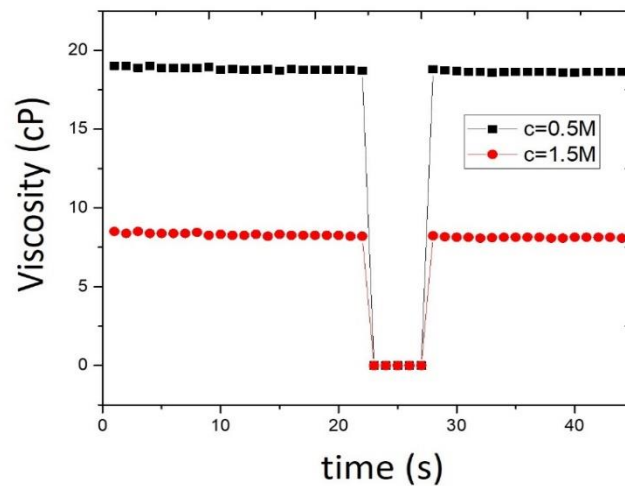
### Summary

During the first reporting period the activities were focused on the planarization of flexible ceramic substrates. These activities consisted in the synthesis and characterization of the precursor solution for the chemical solution deposition of the planarization layers (A1.1), the deposition and optimization of the deposition process of the planarization layers via spin coating (A1.2) and dip coating (A1.3) and the morphological characterization of the planarization layers (A1.4). For the present reporting period, there have been issues regarding the purchase of flexible YSZ ceramic substrates, since the company (ENrG, USA) from which these substrates were planned to be purchased closed its operations. In view of these unforeseen circumstances, until a suitable source for polycrystalline thin/flexible ceramic substrates, we have concentrated our activity on the activity A2.7/A2.8 regarding the deposition of YBCO thin films by chemical solution deposition.

# 1. Solution deposition planarization of flexible, ceramic YSZ substrates

## A1.1 Coating solution synthesis and characterization

For the precursor solution preparation, yttrium acetate,  $Y(CH_3COO)_3 \cdot 4H_2O$ , was dispersed in methanol,  $CH_3OH$ , and dissolved in propionic acid,  $C_2H_5COOH$ . The concentration of the as-prepared solutions was 0.5 M and 1.5 M, respectively. The rheologic properties of the as obtained solutions were investigated. The solution viscosity was determined using a DV1-Brookfield viscosimeter. The minimum solution volume for viscosity determination was 0.5 ml. The results obtained on the two



Fig

solutions is presented in figure 1.1. As was expected the viscosity increases with solution concentration from 8.5 cP to 19 cP. Besides the concentration of the solution, viscosity is also influenced by the solvent content. It may be seen that there is little time variation of the viscosity around the mean value. This is an indication of the stability of the forces that sustain molecular agitation, which is desirable for keeping a high substrate wetting degree. The variation of the shear stress was investigated as a function of the shear rate for the  $c = 0.5$  M solution. The linear dependence of the shear suggests a Newtonian fluid behavior of the precursor solution. The proportionality constant of the two physical quantities, which is the dynamic viscosity,  $\eta$ , was determined to be  $\sim 0.18$  ( $\text{dyn}/\text{cm}^2$ )-s.

The wetting angle of the precursor solution was measured with an Ossila Contact Angle Goniometer, in a static regime. Within the same measurements, the surface tension of the solutions

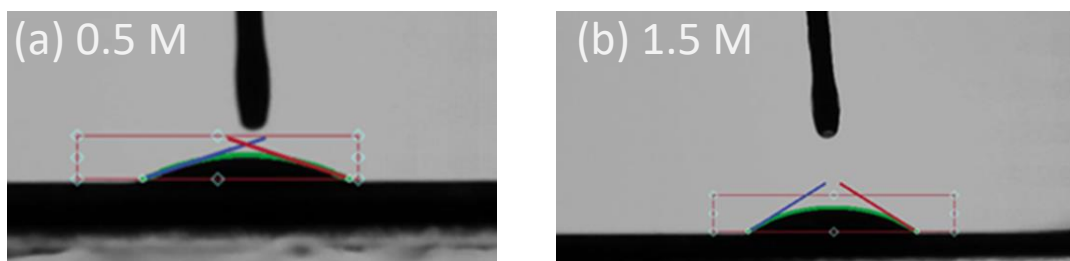


Figure 1.2 Wetting angle determination of the (a) 0.5 M and (b) 1.5 M precursor solutions.

was also evaluated. The results are presented in figure 1.2. The obtained results are summarized in table 1.1. It may be seen that for the 0.5 M solution the wetting angle is quite low, 18.38°, indicating excellent wetting properties of the solution. Even the larger value, 32.2°, measured for the 1.5 M, suggests good prospects for a uniform substrate coating of the precursor solution.

*Table 1.1 Contact angle and surface tensions of the precursor solutions.*

<i>Solution concentration (M)</i>	<i>Contact angle (°)</i>	<i>Surface tension (mN/m)</i>
0.5	18.38	25.3
1.5	32.2	40.8

### A1.3 Optimization of the double-sided deposition process by dip-coating

The present work package has the main objective the planarization of flexible ceramic substrates using a sequence of  $Y_2O_3$  layer deposition. Due to issues concerning the commercial availability of flexible ceramic substrates, 0.15 mm thick,  $Al_2O_3$  (Kerafol, Germany) substrates were used for preliminary planarization studies. The  $Y_2O_3$  layers were grown by the chemical solution deposition method. The precursor solution was deposited on the alumina substrates by dip-coating. After the full substrate immersion in the coating solution, the samples were drawn at a constant rate of 1 mm/s. The as-obtained films were subjected to a thermal treatment, that was performed at 800

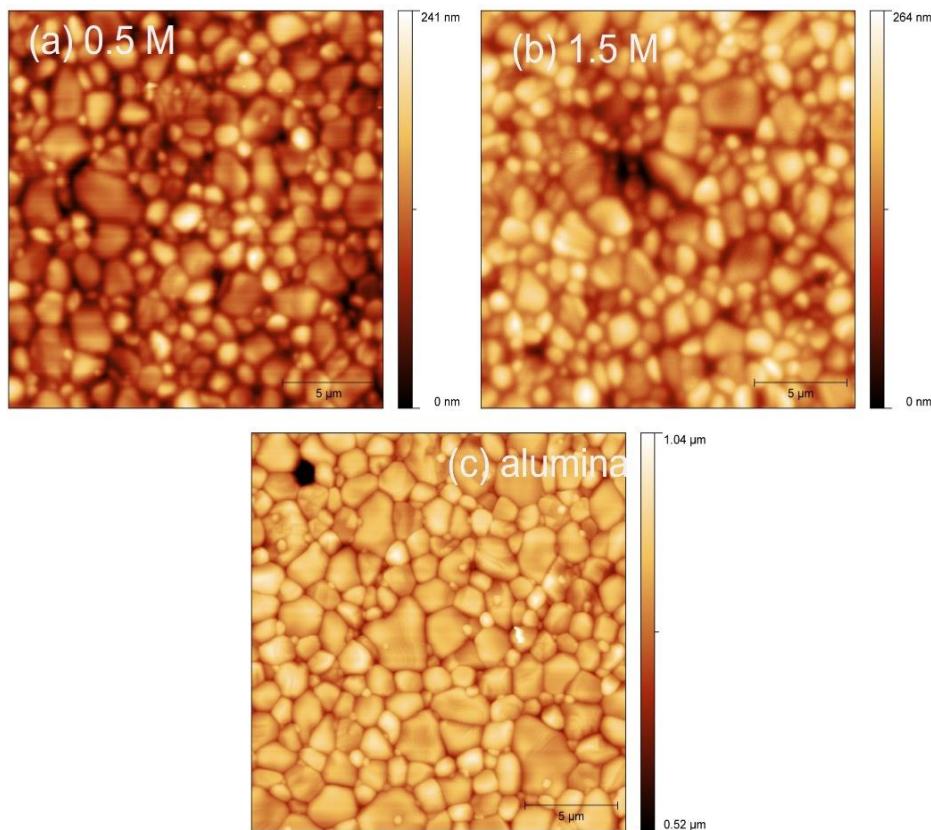


*Figure 1.3.4 20 μm × 20 μm AFM images of the yttria planarization bi-layers obtained from the (a) 0.5 M and (b) 1.5 M solution concentrations. (c) Alumina substrate reference.*

°C in oxygen atmosphere. The reason for this relatively high treatment temperature is to ensure that the subsequent thermal treatments of the following oxide layers, culmination with the  $\text{YBa}_2\text{Cu}_3\text{O}_7$ , which is treated in the range between 815 °C and 835 °C, do not affect the stability of the layers. Since the planarization layer structure constitute the thickest element of the final heterostructure, its thermal stability is paramount for the subsequent film growth.

#### A1.4 Morphologic characterization of the planarization layers

The morphology of the planarization films was investigated using a Veeco Dimension D3100 atomic force microscope. The investigated samples consisted of a  $\text{Y}_2\text{O}_3$  thin films obtained using both the 0.5 M and the 1.5 M precursor solution. Two layers for each sample were deposited by dip-coating (1 mm/s withdrawal rate). After the first deposition the as-obtained films were dried at 100 °C. After the second layer deposition, the bi-layers were annealed at 800 °C in oxygen atmosphere for 1 hour. The obtained results are presented in figure 1.3. The morphological parameters are summarized in table 1.2.

*Table 1.2 Morphological properties of the planarization layers.*

<i>Sample</i>	<i>RMS roughness (nm)</i>	<i>Maximum height (nm)</i>	<i>Average height (nm)</i>
Alumina substrate	58	1148	841
$\text{Y}_2\text{O}_3$ (c = 0.5 M)	34.3	253	111.9
$\text{Y}_2\text{O}_3$ (c = 1.5 M)	35.7	264.5	145.9

It may be observed that even with just two coatings the morphological properties of the planarization layers are dramatically improved with respect to the alumina reference substrate, with a decrease of about 40 % of the RMS roughness and a reduction of the average height by 7.5 times, in the case of the 0.5 M film. Similar values are obtained for the 1.5 M film. Thus, so far, it may be concluded that the yttria films indeed act as a planarization layer, even though several additional coatings are needed to further improve the surface quality. No significant difference is observed when using different concentrations of the precursor solution concentration.

#### Results and perspectives

For the present activity we may conclude that the main foreseen results were achieved:

- the synthesis and characterization of the planarization slution;
- deposition of planarization layers;
- improved morphological properties of the planarized surface.

Due to the afore mentioned set-back, the activity regarding the spin coating deposition of the planarization layer needs to be fulfilled. Also, further improvement of the morphological properties is foreseen, after the evaluation of the results obtained in the next reporting period for the oriented MgO buffer layers.

## 2. YBCO thin film deposition (A2.7/8)

We proposed a novel fluorine free coating solution with added diethanolamine as a chelating agent. The as-obtained results were sent for publication with the title “Investigation of diethanolamine (DEA) as a chelating agent in the fabrication of fluorine free propionate route  $\text{YBa}_2\text{Cu}_3\text{O}_7$  (YBCO) thin films” Andrada Daniel, Mircea Nasui, Traian Petrisor Jr., Ramona Bianca Sonher, Andrea Augieri, Cornelia Pop, Anna Palau, Giuseppe Celentano, Lelia Ciontea and Traian Petrisor. In the following paragraphs we will present the obtained results, following the structure of the afore mentioned article.

### 2.1 Experimental

The YBCO fluorine free coating solution was prepared using cost effective metal acetate precursors  $\text{Y}(\text{CH}_3\text{COO})_3 \cdot 4\text{H}_2\text{O}$ ,  $\text{Ba}(\text{CH}_3\text{COO})_2$ ,  $\text{Cu}(\text{CH}_3\text{COO})_2$  (Alfa Aesar, Germany) in a stoichiometric ratio  $\text{Y}^{3+} : \text{Ba}^{2+} : \text{Cu}^{2+} = 1:2:3$ . Afterwards, the precursors were individually dissolved in methanol (Alfa Aesar, Germany) and propionic acid (Alfa Aesar, Germany). For the  $\text{Ba}(\text{Ac}_2)$  and  $\text{Cu}(\text{Ac}_2)$  mixture,  $\text{NH}_4\text{OH}$  32% (Merck, Germany) was added dropwise until the solution became clear. All these procedures were performed in an ultrasonic bath. In the next step, the solutions were mixed together, stirred for 10 minutes and concentrated by evaporation. The water was evaporated at 75 °C and methanol at 58 °C by using a Büchi R215 rotary evaporator. After the evaporation process, the obtained blue marine coating solution was cooled down to room temperature until the next day. Subsequently, 10% vol. of diethanolamine (DEA, >99%, Fluka, Switzerland) was separately added to improve the solution viscosity and stability. The precursor solutions concentration was 1.1 M. Finally, the solution was deposited by the spin coating method (VTC-100 Vacuum Spin Coater) on 7.5mm × 7.5mm  $\text{SrTiO}_3$  (STO) substrate at a 3000 rpm for 60 s. An important step for a quality coating and surface wettability is the cleaning process of the substrate surface. Cleaning has been performed by sonicating the substrate for 3 minutes in an aqueous solution of nitric acid, followed by 1 minute in isopropanol. After coating, the amorphous film has been subjected to an optimized double-step thermal treatment process. The films were pyrolyzed in a tubular furnace, the temperature was increased from room temperature up to 600 °C with a dwell time of 60 minutes, in humid  $\text{O}_2$  flow (20 l/hour). Subsequently, the YBCO growth took place at 835 °C at a heating rate of 20 °C/min, for 180 min in a humid  $\text{N}_2/\text{O}_2$  atmosphere. The orthorhombic symmetry is developed during the oxygenation at 450 °C on the cooling ramp by maintaining the sample at this temperature for one hour in an oxygen flow.

The thermal decomposition of the precursor powder was performed using thermogravimetric-differential thermal analysis (TG-DTA) coupled with quadrupole mass spectrometry (QMS 200) atmospheric sampling system (Residual Gas Analyzer RGA-Stanford Research System) to reveal the gas species involved during decomposition with  $m/z=10-90$  a.m.u. The analysis was carried out in a humid  $\text{O}_2$  atmosphere up to 800 °C. The powders were obtained by drying the coating solutions on a hot plate

between 50-70 °C. The temperature is adapted to the nature of the added chelating agent. Next, the powder was kept for one hour under vacuum in a dry oven at 70 °C, afterwards grinded in a mortar and pestle. Alumina was used as the reference material.

Infrared analyses of precursor solutions were performed by Fourier Transform Infrared Spectroscopy (FTIR, Bruker Tensor 27) in the range between 500 and 2000  $\text{cm}^{-1}$  with a resolution of 4  $\text{cm}^{-1}$  with 32 scans for each sample.

The structural characterization of the YBCO thin films was performed by X-ray diffraction,  $2\theta/\omega$  and  $\omega$ -scans, using a Bruker D8 Discover diffractometer (Cu  $K\alpha$  radiation). The electrical characterization of the superconducting properties ( $R(T,B)$ ,  $J_c(T,B)$ ) was performed in a Cryogenic Ltd. cryogen-free cryostat in the 4.5-77 K and 0-18 T temperature and magnetic field interval, respectively. For I-V transport measurements films were patterned using standard UV photolithography and wet etching to obtain 1 mm long strips with a width of 30 and 50  $\mu\text{m}$ . The critical current density was estimated from the  $V(I)$  characteristics using a 1  $\mu\text{V}/\text{cm}$  criterion. Magnetization measurements were performed by SQUID (Quantum Design, San Diego, CA) and the Bean critical state model was used to extract the critical current density of the film.

The morphological properties of the film were analyzed by optical microscopy (Zeiss), and atomic force microscopy (AFM-Vecco). The microstructure of the thin film was identified by transmission electron microscopy (TEM), using a JEOL JEM-2100F microscope operated at 200 kV. For TEM sample preparation we used a HELIOS NanoLab 600 instrument, with cutting, thinning, and polishing with a gallium liquid metal ion source at 30 kV acceleration voltage and different probe currents (21 nA, 6.5 nA, and 28 pA). Finally, the resulting TEM lamella dimension is approximately: length = 8 – 10  $\mu\text{m}$ , width = 5 – 6  $\mu\text{m}$ , and thickness = 60 – 100 nm.

## 2.2 Infrared spectroscopy characterization of the precursor solution

To reveal a possible reaction of the organic additive with the YBCO precursor solution, we have performed the FT-IR measurements presented in Fig. 2.1. The stretching vibrations at 1541, 1412, and 1284  $\text{cm}^{-1}$  are characteristic to the asymmetric  $\nu_{(\text{as})}$ , symmetric  $\nu_{(\text{s})}$  carboxylic groups  $\nu(\text{COO}^-)$  to  $\nu\text{CH}_2$ , respectively. Moreover, the coordination mode of the propionate groups can be deduced from the difference of the asymmetric and symmetric absorption of  $\nu(\text{COO}^-)$  [ $\Delta\nu = \nu_{\text{as}}(\text{COO}^-) - \nu_{\text{s}}(\text{COO}^-)$ ]. In our case, the difference  $\Delta\nu = 129 \text{ cm}^{-1}$  indicates a bidentate chelating ligand which binds one or two cations. The presence of this structure makes the solution more robust, by hindering the coordination of water molecules. The peak groups appearing at 1461 and 1020  $\text{cm}^{-1}$  are the characteristic vibration modes of the methyl groups, attributed to  $\text{CH}_3$  and  $\text{CH}_3\text{O}$  radicals. The characteristic band of free carboxylic acid  $\nu(\text{C}=\text{O})$  occurs at 1709  $\text{cm}^{-1}$ , and  $\nu\text{CH}_2\text{-CO-O}$  appears at 1220  $\text{cm}^{-1}$ . The absorption peaks below 650  $\text{cm}^{-1}$  are associated with M-O stretching vibrations. Additionally, the band of ammonia is absent from the

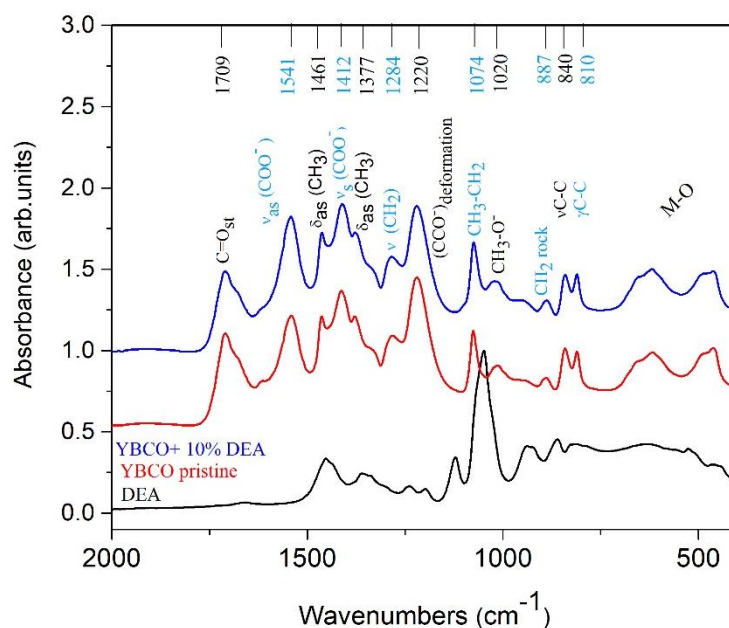


Figure 2.1 FT-IR spectra of the precursor solutions YBCO pristine (red), YBCO+10%DEA (blue) and DEA (black).

spectrum of the precursor solution due to the evaporation process (see experimental methods). The peaks were assigned based on previous literature studies. The spectra of the YBCO solution with DEA nearly coincides with the YBCO pristine solution. No modification of the relative intensity of the YBCO-DEA peaks in the 900-400  $\text{cm}^{-1}$  range, demonstrates that no complexation of DEA occurs with the metal ions.

### 2.3 Thermal decomposition of precursor powders

The decomposition behavior was studied by thermal analysis to optimize the thermal treatment profile for the thin film growth. In Fig. 2.2(a) we have plotted the mass variation of the precursor powders (i) with DEA (YBCO-DEA) and (ii) without DEA (YBCO pristine) heated at a 10  $^{\circ}\text{C}/\text{min}$  heating rate in humid oxygen atmosphere. It can be seen that the samples exhibit an almost similar pattern of the TG profile. The mass loss evolution has revealed that the decomposition occurs in three successive stages. This is also confirmed by the three peaks present in the DTA spectra, Fig. 2.2(b), which occur at different temperatures for the two samples. In the first stage, between 47-187 $^{\circ}\text{C}$  the process displays a single endothermic peak for both samples at 41 $^{\circ}\text{C}$  (YBCO pristine) and 47 $^{\circ}\text{C}$  (YBCO-DEA), respectively, associated with the adsorbed water evaporation, according to the QMS measurements presented in Fig. 2.2(b) for the sample with DEA. From the initial weight, this corresponds to a 4% weight loss.

The second stage, registered in the 187-350  $^{\circ}\text{C}$  temperature range, is equivalent to a mass loss of 31 % for the pristine powder, and 36 % for YBCO-DEA, respectively. The DTA curve shows an exothermic effect at 270 $^{\circ}\text{C}$  (YBCO-DEA), and 282 $^{\circ}\text{C}$  (YBCO pristine). In the case of YBCO-DEA, this step



is attributed to the boiling point of DEA, and also related to the complete chelating process (with loss of gaseous NO<sub>x</sub>).

The complete decomposition reaction occurs by forming CO<sub>2</sub>, NO<sub>2</sub> and H<sub>2</sub>O volatile products. However, the high boiling point may promote a higher polymerization degree. Different degree of

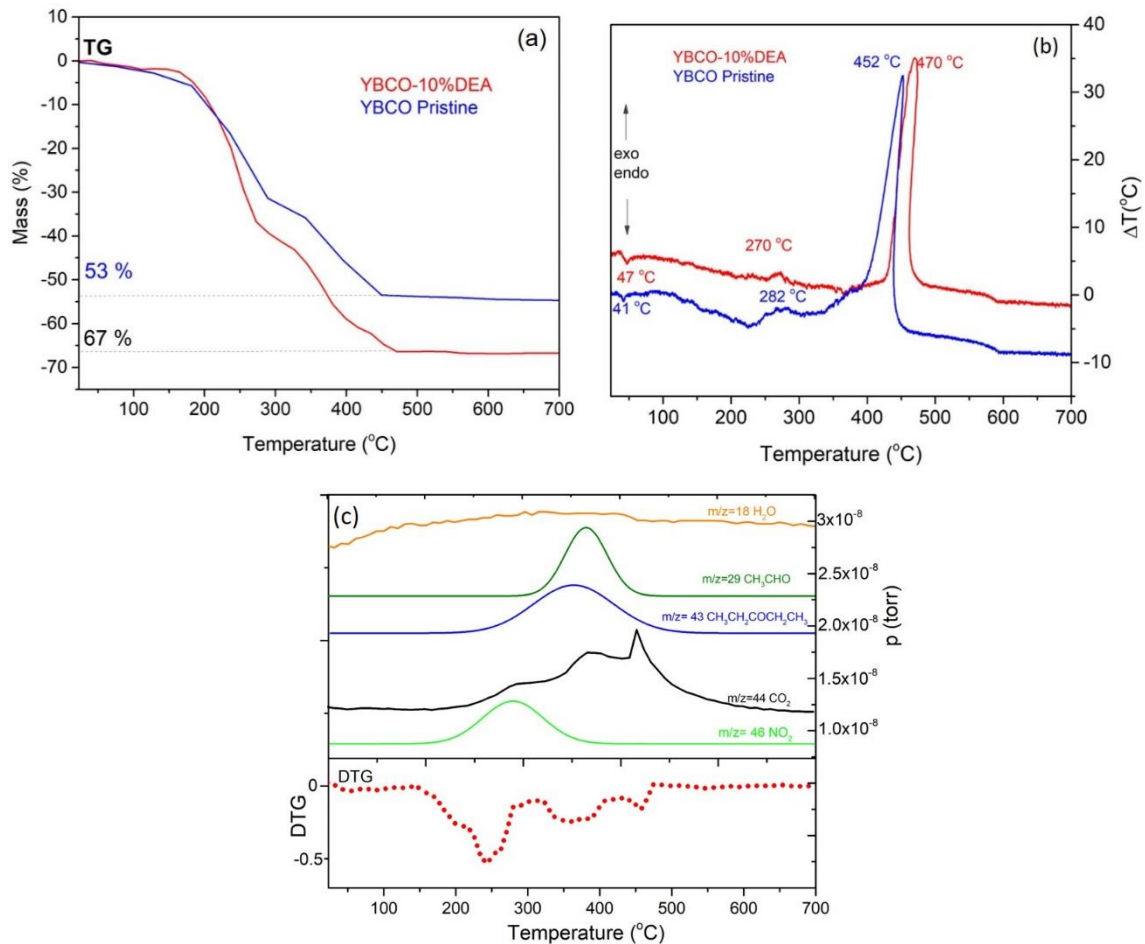


Figure 2.2 (a) TG and (b) DTA during decomposition at 10°C/min in humid O<sub>2</sub> atmosphere, and (c) the corresponding MS spectra of solid powder with DEA (YBCO-DEA).

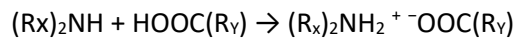
polymerization due to the molecules of the chelating agents can affect the pyrolysis process of the thin films, which is the transformation of gels in an amorphous state. This can be explained in terms of nucleation and growth process.

The third stage (390- 600°C) is related to the precursors' decomposition evidenced by the exothermic peaks between 452-470°C. The fact that the peaks of the DEA- chelated precursor shift to higher temperature may demonstrate that the DEA solution has a chemical bonding to propionate groups. The total weight loss was 53% for pristine and 67% for YBCO-DEA, respectively. According to the TG curves the difference of the weight loss can be associated with the decomposition of metallic propionate. In the case of YBCO-DEA the MS (Fig. 2.2b) has revealed that the evolved gases correspond to the fragments with m/z= 43 characteristic for 3-pentanone (CH<sub>3</sub>CH<sub>2</sub>COCH<sub>2</sub>CH<sub>3</sub>), m/z= 29 for CH<sub>3</sub>CHO



and  $m/z = 44$  for  $\text{CO}_2$ . All these fragments correspond to the propionate decomposition [28]. After the precursor decomposition, above  $600^\circ\text{C}$  the weight loss of the powder remains stable.

Precise elucidation of the decomposition process is hindered by the presence of three metal ions participating in the chelating process, with different ionic radii,  $r$ . These are  $1.61\text{\AA}$ ,  $0.87\text{\AA}$  and  $0.99\text{\AA}$  for  $\text{Ba}^{2+}$ ,  $\text{Cu}^{2+}$ , and  $\text{Y}^{3+}$ , respectively. The reactivity of metal cations in the formation of metal-chelate complexes may be influenced by the large differences in the ionic. Generally, the possible reaction between amine and carboxylate complex can be expressed as follows:



where  $\text{R}_x$  is the alkyl substituent into the amine compound (ethyl or butyl).  $\text{R}_y$  is the alkyl substituent into the acid compound (propyl, hexyl, or heptyl). In this work, diethanolamine (DEA) was used as the source of the cations, while carboxylate acids with alkyl chain length of propyl, was utilized to provide the anions of the complex.

## 2.4 Structural and morphological characterization

The physical properties of the as-obtained YBCO – 10 vol. % DEA thin films were investigated to assess the efficiency of the proposed approach in producing high performance superconducting YBCO thin films. The  $2\theta/\omega$  diffraction pattern of the film is presented in Fig. 2.3(a). It may be observed that the expected (001) texture of the YBCO film is present. Common issues affecting YBCO film epitaxy are the growth of crystallites oriented with the  $a/b$  axes perpendicular to the substrates, or poor overall film texture. These determine the presence of ( $h00$ ) and (103) peaks, respectively in the X-ray pattern. No such features were observed in our measurement, as no additional peaks, besides the (00 $l$ ) family, were recorded from the YBCO film. The out-of-plane  $c$  lattice parameter was evaluated using the Nelson-Riley method, to be  $11.67\text{\AA}$  typical for YBCO thin films grown on STO (001) substrate. The lower value of the out-of-plane constant than its powder counterpart,  $11.6802\text{\AA}$ , may be ascribed to the in-

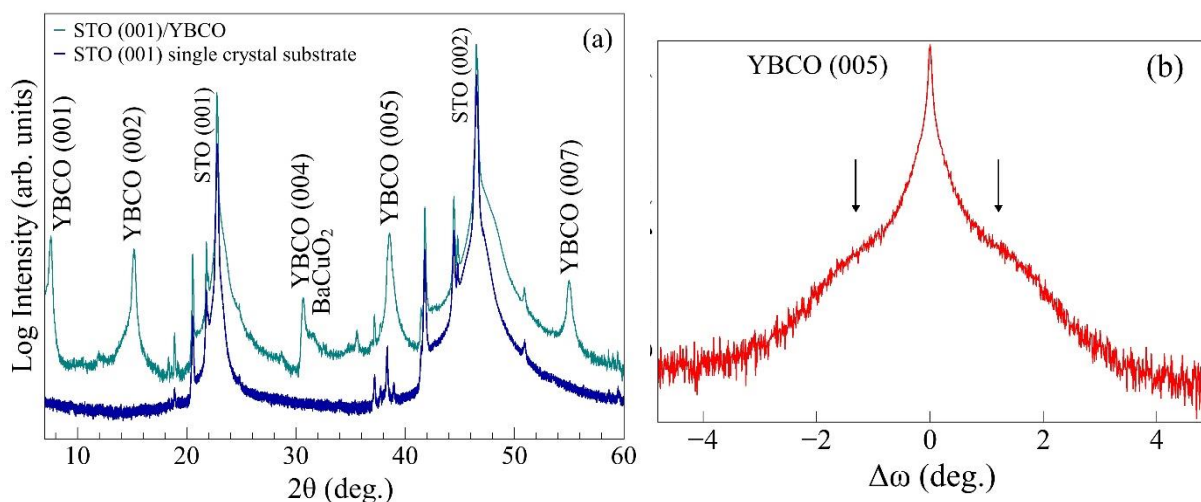


Figure 2.3 (a)  $2\theta/\omega$  pattern for the YBCO thin film and the STO (001) single crystal substrate; (b)  $\omega$ -scan around the YBCO (005) reflection (arrows mark the diffuse scattering peaks).

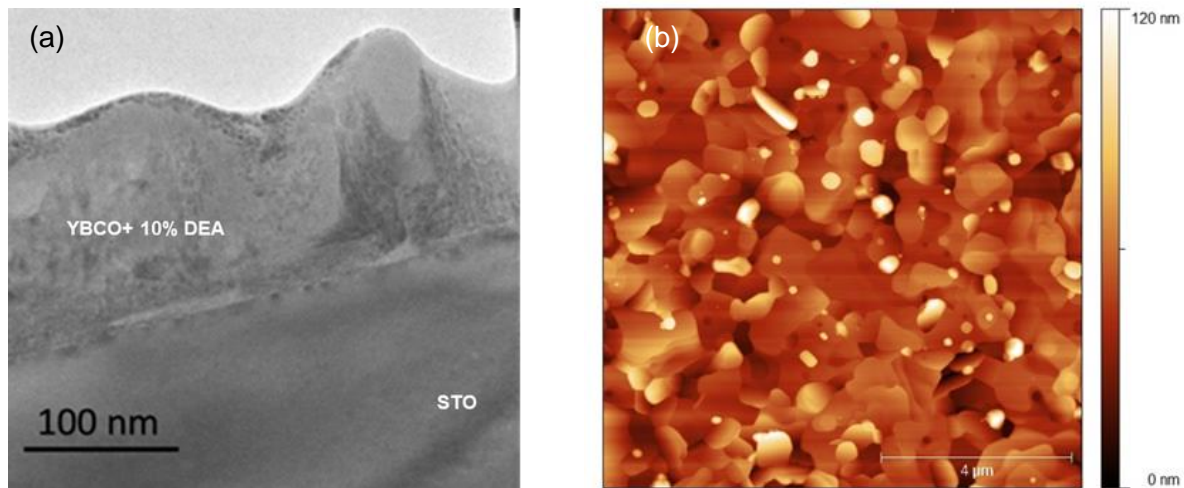


Figure 2.4 (a) TEM image and (b)  $10 \times 10 \mu\text{m}$  AFM image of YBCO-10 vol%.DEA film.

plane tensile strain present in the film. The cubic STO lattice constant is  $3.905 \text{ \AA}$ , larger than both  $a$  and  $b$  parameters of YBCO leading to a mismatch of 1.56 %. Additional  $\text{BaCuO}_2$  secondary phase was identified. For comparison, the X-ray diffraction pattern of the bare STO (001) single crystal substrate was added. The out-of-plane crystallite mosaicity was evaluated by performing an  $\omega$ -scan around the YBCO (005) reflection, figure 2.3(b). The full-width at half-maximum (FWHM) of the as-obtained curve is  $0.09^\circ$ . The low value of the FWHM indicates a very narrow out-of-plane crystallite orientation distribution function. However, it may be observed that there is an additional, low intensity contribution, to the rocking curve, present in the form of symmetric shoulders, indicated by the arrows. In oxide epitaxial systems, such features are common. They may be explained on one hand by the existence of coherent diffraction on highly textured crystallites, responsible for the narrow high intensity peak. On the other hand, there is a diffuse X-ray scattering on local strain fields present around structural defects, which accounts for the low intensity component. The thickness of the as-obtained film was determined by means of transmission electron microscopy (TEM). The TEM image, Fig. 2.4(a), suggests a rather high thickness variation, with a minimum thickness of approximately 90 nm. The film is dense and shows a crack-free surface.

The surface morphology was investigated by contact AFM measurements on a  $10 \times 10 \mu\text{m}^2$  area, Fig. 2.4(b). The surface morphology exhibits large flat crystallites with pores which may extend to the substrate surface. The presence of the large regular crystallites indicates a good crystallinity of the YBCO film, which, corroborated with XRD data demonstrated a good quality of the as-grown epitaxial YBCO film. Additionally, smaller round shape particulates grains are also visible. These are most likely amorphous phases such as:  $\text{CuO}$ ,  $\text{Y}_2\text{O}_3$ , etc. Quantitatively, the root-mean-square (RMS) roughness was estimated to be 14 nm, while the peak-to-valley distance was  $>120 \text{ nm}$ .

## 2.5 Superconducting transport properties

The temperature and magnetic field dependence of the resistivity,  $\rho(T, H)$ , of the YBCO film was studied near the critical transition temperature,  $T_c$ . The results are presented in Fig. 2.5. In zero magnetic field, the zero-resistance critical temperature,  $T_c(R=0)$  is 88.1 K. The observed temperature-magnetic field dependence of the electrical resistivity is interpreted with the model of the thermally activated flux flow (TAFF), which well describes the broadening of the resistive transition and the decrease of  $T_c$  with the increase of the applied magnetic field. In the TAFF regime, for small current densities,  $J \ll J_c$ , the resistivity decreases exponentially as a function of temperature, according to

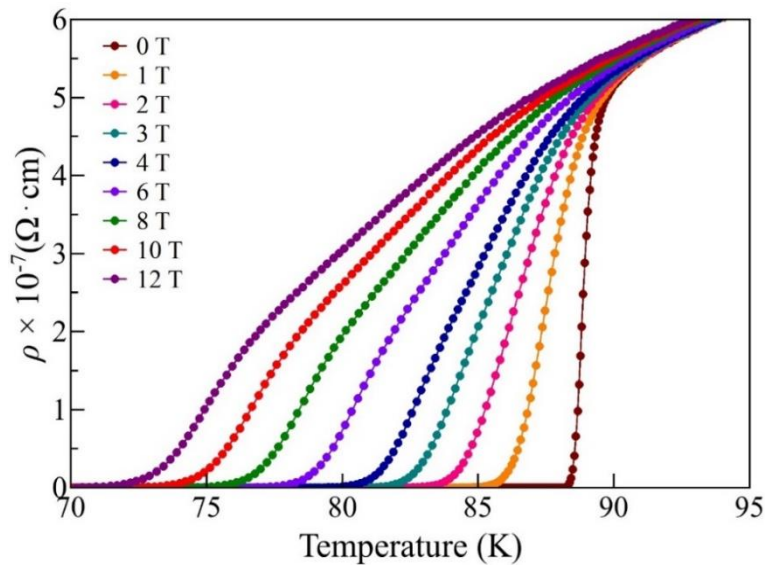


Figure 2.5  $\rho(T)$  of YBCO thin film for various values of magnetic field showing the broadening of the resistive transition by magnetic field.

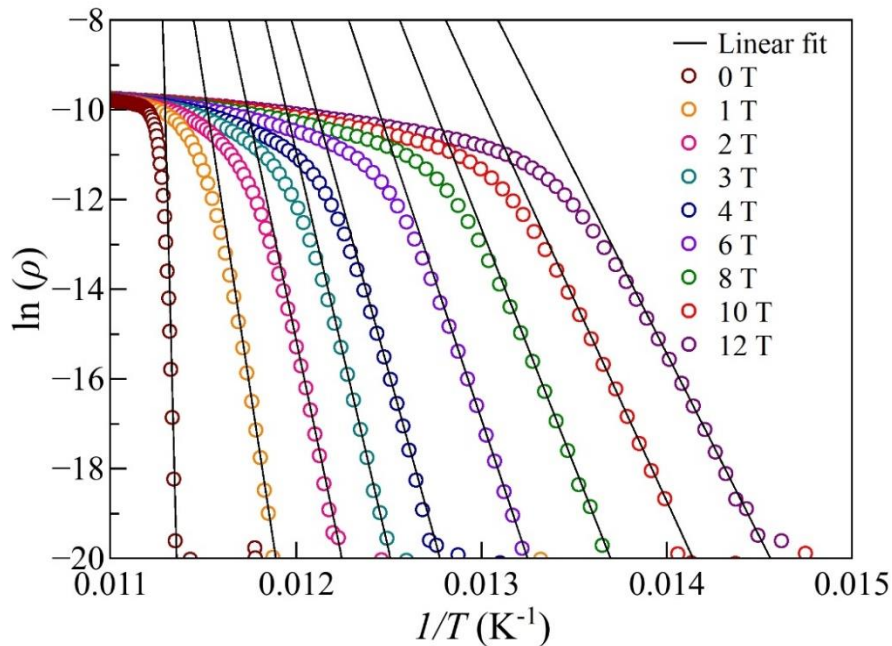
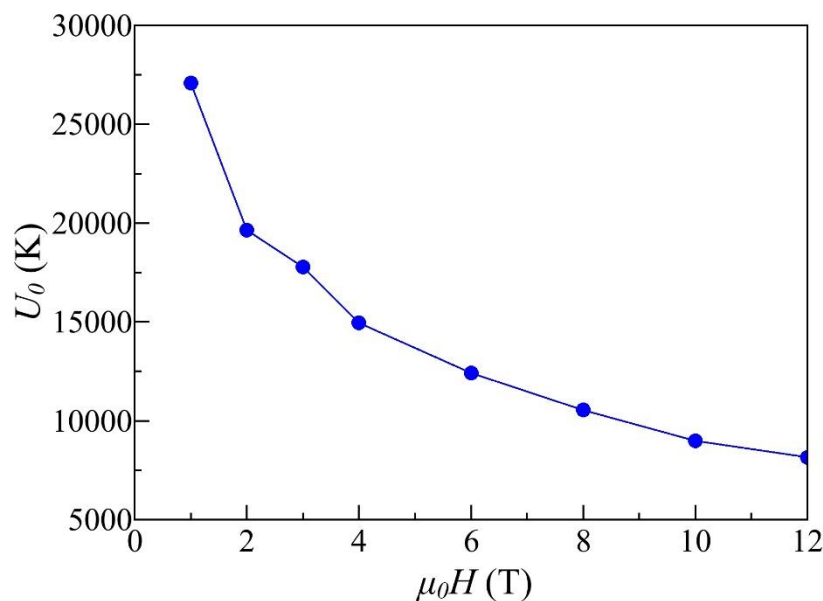


Figure 2.6 Linear fit of the  $\ln(\rho)$  vs.  $1/T$  dependencies.

$\rho(T, H) = (2\rho_c U/T) \exp(-U/T) = \rho_{0f} \exp(-U/T)$ .  $U$  is the thermal activation energy (TAE), while the  $2\rho_c U/T$  pre-factor is usually considered to be a constant, noted as  $\rho_{0f}$ . Usually, to calculate  $U_0$ , the  $\rho(T)$  data is plotted in an Arrhenius form  $\ln(\rho)$  vs.  $1/T$ . The TAFF regime is situated in the linear part of the as obtained dependence.  $U_0$  is determined as the slope of the linear regression of the experimental data, while the  $y$ -axis intercept is  $\ln(\rho_0)$ . As it may be seen from Fig. 2.6, a linear dependence of  $\ln(\rho)$  as a function of  $1/T$  is observed in the TAFF regime. From the absolute values of the linear regression (solid lines), the slope  $U_0$  was determined. In Fig. 2.7. the magnetic field dependence of the thermal activation energy is presented. The lack of additional pinning sites determines a rather steep decrease of the activation energy as a function of the applied magnetic field, especially at low fields.

One of the most important parameters in determining the superconducting transport performance is the critical current density,  $J_c$ . Its absolute value, together with its magnetic field and temperature dependence give a comprehensive image of the current carrying capabilities of a certain superconducting architecture. In Fig. 2.8, the magnetic field dependence of the  $J_c$  is presented at several temperatures. For comparison, the  $J_c(\mu_0H)$  at 77 K determined both by  $V(I)$  and magnetic SQUID measurements is shown. Transport measurements reveal a critical current density value in self-field of 3 MA/cm<sup>2</sup>, while a slighter higher value, ~4 MA/cm<sup>2</sup>, is registered from magnetization determination. The field dependencies of the two curves are relatively similar, both showing a steep decrease of the critical current density with the increase of the applied magnetic field. Since the magnetization measurements were performed on the entire sample, while the  $V(I)$  measurements were performed on patterned stripe, the similarity of the two magnetic field dependencies is an indication of the good



**Figure 2.7** Thermal activation energy,  $U_0$ , as a function of the applied magnetic field.

homogeneity of the as-obtained film. The maximum pinning force density,  $F_p^{max}$ , was 0.95 GN/m<sup>3</sup>, determined from transport measurements and 0.64 GN/m<sup>3</sup> from magnetization measurements ( $F_p = J_c \times \mu_0 H$ ). No satisfactory fit was obtained for the data at 77 K using the power law decay,  $J_c \propto H^{-\alpha}$ . This may be ascribed to a low irreversibility field value,  $H_{irr} = 2.2$  T (determined as the field at which the

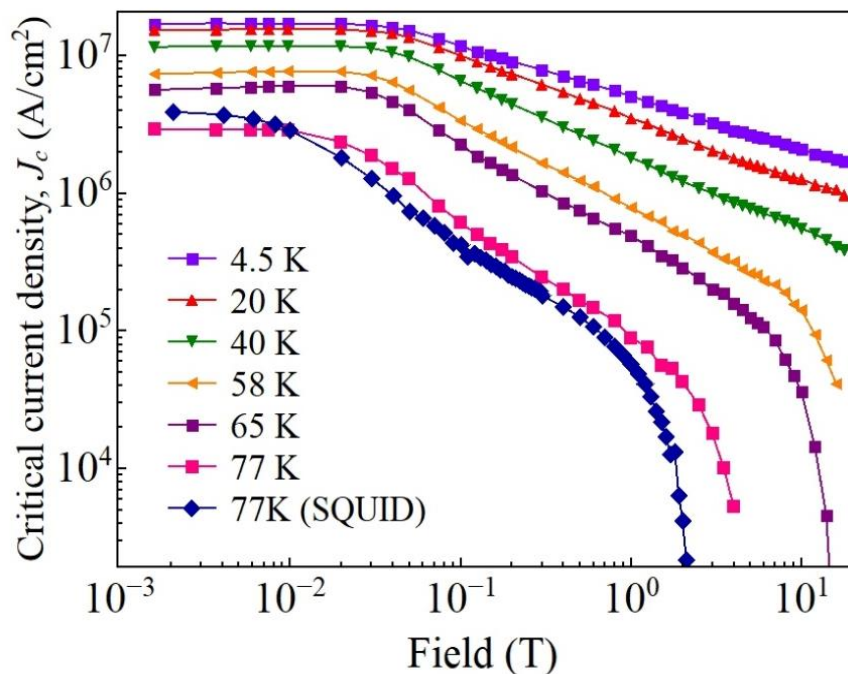


Figure 2.8 Magnetic field dependence of the critical current density at different temperatures

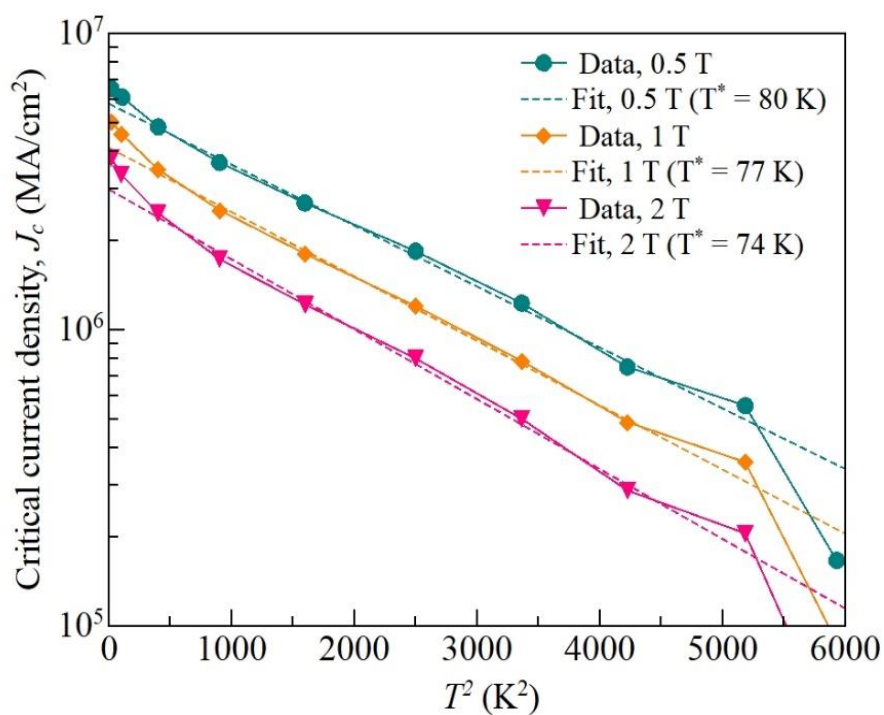


Figure 2.9  $J_c(T^2)$  dependencies at different applied magnetic fields, with the appropriate fits for the characteristic vortex pinning energy,  $T^*$  determination.

normalized pinning force decrease below 0.01), which in turn can be a result of the relatively low critical temperature. As expected, with the decrease of the temperature, thermal activation of the vortices is reduced, determining an increase of the critical current density in all the studied field range. At 4.5 K, for fields higher than 0.1 T, the power law describes well the  $J_c(\mu_0 H)$  curve, with an exponent  $\alpha = 0.35$ . The low  $\alpha$  value indicates that at low temperatures the film exhibits good vortex pinning properties. The above results suggest that the intrinsic occurring pinning centres within the film fail to provide sufficient pinning strength at high temperatures, *i.e.*, 77 K, but at the same time prove to be more effective in the low temperature range. Among the intrinsic pinning centres, the most important are point defects and twin boundaries. Due to the short coherence length in the HTSC the defect at a single atom site is sufficient to depress locally the superconducting parameters and, as a result, to act as efficient pinning centres. In an epitaxial YBCO film, the most common point defect is represented by the oxygen deficiency in the  $\text{CuO}_2$  planes. It is to be noted that the density of this defect is strongly dependent by the film growth conditions.

The evolution of the critical current density as a function of the sample temperature was investigated at different magnetic fields ( $H \parallel c$ ) to assess the nature of vortex pinning present within the film. It has been shown that three types of pinning contributions may exist in epitaxial YBCO thin films classified according to their strength and direction of action. These are isotropic weak, isotropic strong, and anisotropic strong centres. The weak and strong contributions have specific temperature dependencies. In case of the strong populations the analytical expression for the critical current density is  $J_c(T) \sim J_c(0) \exp(3(T/T^*)^2)$ , where  $J_c(0)$  is the critical current density at 0 K, while  $T^*$  is a characteristic vortex pinning energy. In Fig. 2.9 the  $J_c$  is presented as a function of  $T^2$ , in logarithmic scale, at different applied magnetic fields. The data was fitted with the above expression, and it may be observed that for all investigated fields it closely follows the respective fits in the 20 – 65 K interval. This means that in the specified temperature regime the dominant contribution comes from a strong pinning population. The as-obtained  $T^*$  values started at  $\sim 80$  K at 0.5 T and decreased to  $\sim 74$  K at 2 T.. This contribution becomes dominant at high magnetic fields. The satellite peaks in the rocking curve pattern, confirm the existence of such correlated lattice defects and therefore explain the observed strong pinning contribution. However, it is to be noted that ascribing the strong pinning population to twin boundaries is a hypothesis, since no direct evidence of their presence is evidenced. At lower and higher temperatures there is a deviation from the fit. At low temperatures  $< 10$  K, the dominant pinning population is the isotropic weak population, generally associated with point defects such as oxygen vacancies or atomic inclusions.



## Results and perspectives

The influence of diethanolamine used as a chelating agent in the preparation of YBCO fluorine free propionate chemical solution has been investigated. IR measurements have shown that DEA appears not to form a new complex, although complexation might differ depending on the pH value. Thermal decomposition studies for the YBCO and the YBCO-DEA precursor powders revealed their similar decomposition behavior, corresponding to a multistep mass loss with the liberation of CO<sub>2</sub>, NO<sub>2</sub>, H<sub>2</sub>O and fragments corresponding to the propionate. No polymerization of the metal precursors was revealed, but the formation of bridges between CH<sub>3</sub>CH<sub>2</sub>COO<sup>-</sup> propionate ion groups and DEA may occur through electrostatic attraction. A more detailed analysis is needed to elucidate the nature of the DEA-precursor solution interaction. The as-obtained films, deposited on single crystal SrTiO<sub>3</sub> substrates, show a good epitaxial growth. Secondary peaks present in the  $\omega$ -scan performed on the (005) YBCO peak indicate the presence of a periodicity of structural defects within the film matrix. The thermal activation energy,  $U$ , was determined. Although in self-field at 77 K, a value of  $\sim 4$  MA/cm<sup>2</sup> was measured, the value of  $J_c$  strongly decreased when increasing the magnetic field. On the other hand, at low temperatures, the magnetic field dependence of  $J_c$  is much better, as the power law,  $J_c \propto H^{-\alpha}$ , fit of the data gives a relatively low  $\alpha$  value of 0.35. From the  $J_c(T)$  curves determined at low magnetic fields,  $< 2$ T, with  $H // c$ , we conclude that at intermediate temperatures there is a strong pinning population, which we link to the same defect population responsible for the low intensity satellite  $\omega$ -scan peaks, possibly twin boundaries.

In conclusion, our study demonstrates that the addition of DEA in propionate-based precursor solutions for YBCO thin film deposition has a positive effect on film growth and superconducting transport performance. This result will be used for the subsequent activities, corresponding to the second reporting period. Also, it means the partial fulfillment of activities A2.7 and A2.8.

## 3. Dissemination

Submitted article:

- “Investigation of diethanolamine (DEA) as a chelating agent in the fabrication of fluorine free propionate route YBa<sub>2</sub>Cu<sub>3</sub>O<sub>7</sub> (YBCO) thin films” Andrada Daniel, Mircea Nasui, Traian Petrisor Jr., Ramona Bianca Sonher, Andrea Augieri, Cornelia Pop, Anna Palau, Giuseppe Celentano, Lelia Ciontea and Traian Petrisor (submitted to Ceramics International).

Cluj-Napoca,  
December 2021

Project director,  
dr. Traian Petrișor